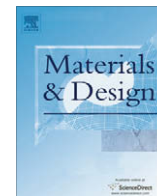




Contents lists available at ScienceDirect

Materials and Design

journal homepage: [www.elsevier.com/locate/matdes](http://www.elsevier.com/locate/matdes)

Short Communication

## Surface residual stress evaluation in double-electrode butt welded steel plates

S.F. Estefen<sup>a</sup>, T. Gurova<sup>a,b</sup>, X. Castello<sup>a</sup>, A. Leontiev<sup>c,\*</sup><sup>a</sup>Subsea Technology Laboratory, COPPE, Federal University of Rio de Janeiro, Rio de Janeiro, Brazil<sup>b</sup>GURTEQ, Ensaios Não Destrutivos Ltda, Rio de Janeiro, Brazil<sup>c</sup>IM, Federal University of Rio de Janeiro, Rio de Janeiro, Brazil

## ARTICLE INFO

## Article history:

Received 12 June 2009

Accepted 25 August 2009

Available online xxxxx

## ABSTRACT

Surface residual stress evaluation for double-electrode welding was studied. The stresses were monitored after each operational step: positioning, implementing of constraints, welding and constraints removal. The measurements were performed at the deposited metal, heat affected zone, base metal close to the weld joint and along the plate using the X-ray diffraction method. It was observed differences in the stress evaluations for double-electrode welding which resulted in lower bending distortions and higher values of surface residual stresses, compared with single-electrode welding. This behavior is associated with the stress distribution just after the welding processes in both heat affected zone and base metal close to the fillet for double-electrode welding. The main results from the laboratorial tests indicated lower values of the bending distortions for double-electrode welding compared with the single-electrode. In relation to the residual stress, the double-electrode welding generated, in general, higher stress values in both longitudinal and transversal directions.

© 2009 Elsevier Ltd. All rights reserved.

## 1. Introduction

Welding techniques with multi wires and multiple electrodes appeared in the middle of the past century, providing several technological advantages like welding time reduction and quality of the joint in relation to the conventional multi-pass single-electrode welding [1]. These factors are important for industrial applications, especially in the shipbuilding industry, where the welding process represents 20–30% of the fabrication time and up to 10% of the production cost.

The use of double-electrode welding aims at increasing productivity due to higher deposit rate compared with single-electrode. In addition, the base metal input heat can be maintained relatively low while the conventional single-electrode gas metal arc welding (GMAW) uses a large current for a high deposition rate. Therefore, for the same deposition rate, the double-electrode process is associated with less heat and low base metal current compared to the single-electrode GMAW. Double-electrode welding presents different aspects which have already been investigated, such as process stability, effects of total current and melting rate, microstructure, and heat affected zone (HAZ) hardness [2–4].

Other important parameters are residual stresses and distortions of the welded parts. Residual stresses arising due to welding can have significant influence on the service performance of

welded structural members. Metallurgical processes in welding, such as shrinkage, quenching, and phase transformations, produce both tensile and compressive residual stress in different zones of the welded parts [5]. These residual stresses, particularly tensile stresses, can have important influence on reliability and integrity of the welded components. Tensile residual stresses may result in fatigue cracks, stress corrosion cracking, and other types of fracture. It is important, therefore, to understand the distribution of residual stresses on the surface of the welded components in and near the welding zone. Different factors affect the distribution of residual stresses in welded joints and structures [6]. The principal factors are: residual stresses present in the parts being joined before welding; material properties of the weld and jointed parts; geometry of the parts; applied restrains; welding procedure, including the weld preparation, welding conditions and pass sequence in multi-pass welding; residual stresses generated or relaxed by manufacturing operations after welding or by thermal and mechanical loading during service life. The first analytical models for the residual stresses in welded parts appeared also in the middle of last century [7]. New techniques for measurements, equipment improvements, and advances in computational methods have stimulated several studies based on both numerical and experimental analyses of welding processes [8–10]. Residual stress distribution in multiple electrodes or multi wires electrode welding were obtained from numerical simulation in [11] and [12]. Different sources of residual stresses simulated by computer are very common in the literature, but there is a lack of experimental work

\* Corresponding author. Tel.: +55 21 2562 7505.  
E-mail address: [anatoli@im.ufrj.br](mailto:anatoli@im.ufrj.br) (A. Leontiev).

### Nomenclature

$E$	Young's modulus	$\varepsilon$	elastic strain
$\nu$	Poisson's ratio	$d$	interplanar distance
$\varphi$	azimuthal angle in spherical coordinate system	$\theta$	diffraction angle
$\psi$	polar angle in spherical coordinate system		
$\sigma_\varphi$	measured stress component in $\varphi$ -direction		
$\sigma_1, \sigma_2$	principal stresses		

based on these measurements. To the authors' knowledge, no experimental analysis of the case of double-electrode welding has been made until now.

The main objective of this work is the experimental study of the evolution of GMAW double-electrode welding surface residual stresses and the comparison of these results with multi-pass single-electrode techniques at the butt joined typical ship plates. Single-electrode and double-electrode welding stress distributions are expected to be different, because of the respective thermal regimes, thermal cycles, thermal front extensions, cooling regimes, quantity of melt material and, in consequence, the effects of phase transformations that occur in the deposited metal, HAZ and base metal close to the weld fillet [3].

Surface stress distributions have been measured considering plane stress state. Usually, the residual welding stresses are analyzed in the longitudinal and transversal directions in relation to the weld fillet. This is justified by the fact that the more representative area for the stress analysis is located near the weld fillet, where from the theoretical point of view and under some symmetry assumptions, the longitudinal and transversal directions are the principal stress directions. The stresses were measured by X-ray diffraction method. By this method it is possible to obtain absolute stress values in the deposited metal, HAZ and base metal close to the weld fillet separately.

## 2. Experimental

The experiments were performed using ASTM 131 grade A ferritic steel plates typically employed in the shipbuilding industry. The yield strength of the plate material is 235 MPa and the chemical composition is presented in Table 1.

Each laboratorial test jointed two plates of dimensions 2200 mm × 840 mm × 19 mm, with the chamber angle of 20°. Two specially designed tables have been manufactured in order to support the plates and to provide the clamped conditions during the welding. The plates have been restricted against out-of-plane displacements at the outside edges (lateral constraints), and on the mid-plate along and across the weld line direction using two beams with  $I$  cross-section (internal constraints). Position of the internal constraints is given in Fig. 1 under both longitudinal and transversal symmetry assumptions.

The first pair of plates was jointed with single-electrode welding in four filling layers and 11 steps using MIG (Metal Inert Gas) manual procedure at 3.7 mm/s average speed. Average values of welding current and voltage were 203 A and 27 V, respectively.

**Table 1**  
Chemical composition of plate's material.

Element	Quantity (%)
Carbon	Max. 0.23
Iron	97.0
Manganese	2.73
Phosphorus	Max. 0.05
Sulphur	Max. 0.05

The second pair of plates was welded with double-electrode techniques in three steps of 7 mm, 12 mm and 19 mm thickness. Welding procedure was performed automatically by a magnetic car. Welding data are presented in Table 2. In both cases the employed electrode was 1.2 mm carbon steel rod identified by the specification AWS A5.20 E71T-1 with yield strength 548 MPa.

## 3. Stress measurement methodology

The absolute values of stresses were measured on the top side of the plate surface in longitudinal and transversal directions by X-ray diffraction method using the portable equipment, RAYSTRESS [13], which explores the method of double exposure. This measuring technique was widely tested and successfully employed to different practical engineering applications [14–20].

The RAYSTRESS equipment components, Fig. 2: (1) power and control unit which supplies a high voltage source and control the X-ray tube anode current and voltage; (2) the X-ray tube coupled to a high voltage source. The tube has two air cooled chromium anodes, which emit two convergent X-ray beams for double exposure X-ray stress measurements; (3) a magnetic support to attach the equipment into analyzed surface and to adjust it in the exposure position; (4) a collimator unit with film cassette.

The principles of the double exposure technique used in surface stress measurements with RAYSTRESS equipment are based on the determination of two strain components  $\varepsilon_{\varphi,\psi 1}$  and  $\varepsilon_{\varphi,\psi 2}$ . Let  $\varphi$  and  $\psi$  be azimuthal and polar angles in spherical coordinate system, Fig. 3. Considering the surface stress distribution, let  $\sigma_1$  and  $\sigma_2$

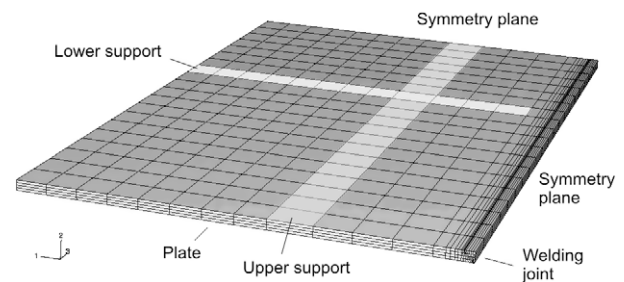


**Fig. 1.** Schematic diagram of the internal constraints position.

**Table 2**  
Double-electrode welding data.

Pass	Electrode	$U$ (V)	$I$ (A)	Speed (mm/s)
1	1	29.17	324.00	7.26
1	2	24.83	231.33	7.26
2	1	27.94	433.40	8.21
2	2	26.14	143.80	8.21
3	1	28.77	353.03	5.08
3	2	24.07	254.34	5.08
3	2	24.07	254.34	5.08

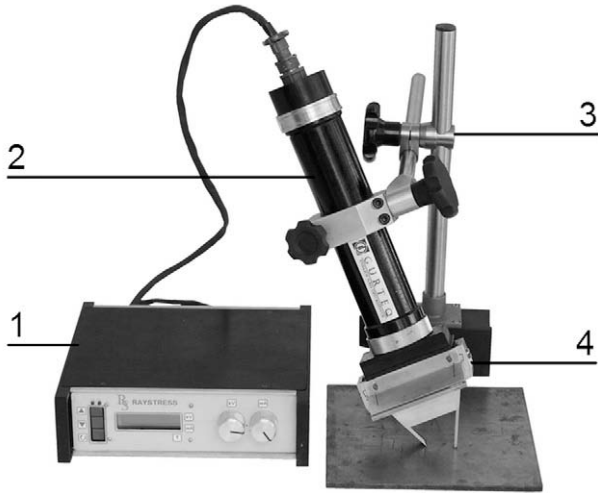


Fig. 2. RAYSTRESS portable equipment.

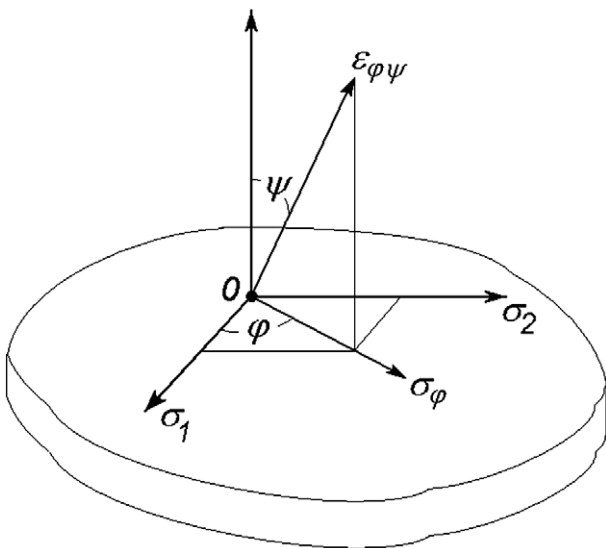


Fig. 3. Orientation of the coordinate system in the specimen surface.

be the principal stresses values and  $\sigma_\varphi$  the stress component in  $\varphi$ -direction. In the specimen surface the third principal stress component is assumed to be zero. Within the framework of isotropic body elasticity theory, for the strain  $\varepsilon_{\varphi,\psi}$  in  $\varphi,\psi$ -direction we have [21]:

$$\varepsilon_{\varphi,\psi} = \frac{1+\nu}{E} \sigma_\varphi \sin^2 \psi - \frac{\nu}{E} (\sigma_1 + \sigma_2), \quad (1)$$

where  $E$  and  $\nu$  are Young's modulus and Poisson's ratio, respectively.

Then the difference between two strain components is:

$$\varepsilon_{\varphi,\psi_2} - \varepsilon_{\varphi,\psi_1} = \frac{1+\nu}{E} \sigma_\varphi (\sin^2 \psi_2 - \sin^2 \psi_1). \quad (2)$$

The stress component  $\sigma_\varphi$  from the expression (2) is equal to the following:

$$\sigma_\varphi = \frac{E}{1+\nu} \left( \frac{\varepsilon_{\varphi,\psi_2} - \varepsilon_{\varphi,\psi_1}}{\sin^2 \psi_2 - \sin^2 \psi_1} \right). \quad (3)$$

Using differentiation of Bragg's law we have:

$$\varepsilon_{\varphi,\psi} = \frac{d_{\varphi,\psi} - d_0}{d_0} = -\text{ctg} \theta_0 (\theta_{\varphi,\psi} - \theta_0), \quad (4)$$

where  $d_{\varphi,\psi}$ ,  $d_0$ ,  $\theta_{\varphi,\psi}$ ,  $\theta_0$  are interplanar distances and diffraction angles for analyzed and free of stress materials, respectively. From expressions (3) and (4) the final formula for the determination of the  $\sigma_\varphi$  stress component may be obtained:

$$\sigma_\varphi = -\frac{E}{1+\nu} \frac{\text{ctg} \theta_0 (\theta_{\varphi,\psi_2} - \theta_{\varphi,\psi_1})}{\sin^2 \psi_2 - \sin^2 \psi_1}. \quad (5)$$

Thus, to determine any surface stress component in  $\varphi$ -direction it is necessary to measure the diffraction angles corresponding to deflection from lattice planes with normals characterized by two angles  $\psi_1$  and  $\psi_2$ . The angular values used in the equipment are  $\psi_1 = 0^\circ$  and  $\psi_2 = 50^\circ$ .

Let  $I_1$  and  $I_2$  be two incident beams with angles  $\psi_1 = 0^\circ$  and  $\psi_2 = 50^\circ$ , and  $R_1$  and  $R_2$  the respective projections of the diffraction cones to the cassette plane, see Fig. 4. For the diffraction angles  $\theta_{\varphi,\psi_1}$  and  $\theta_{\varphi,\psi_2}$  we have:  $\theta_{\varphi,\psi_1} = 0.5(\pi - A_1 \hat{O}B_1)$  and  $\theta_{\varphi,\psi_2} = 0.5(\pi - A_2 \hat{O}B_2)$ .

Thus, the angle difference  $\theta_{\varphi,\psi_2} - \theta_{\varphi,\psi_1}$  can be expressed as

$$\theta_{\varphi,\psi_2} - \theta_{\varphi,\psi_1} = K(B_2 C_2 - B_1 C_1), \quad (6)$$

where  $B_1 C_1$  and  $B_2 C_2$  are the distances from the diffraction lines to the collimator reference marks  $C_1$  and  $C_2$ , and  $K$  is the scale and transfer coefficient from linear units to angle units. The value of the coefficient  $K$  is a characteristic of the cassette-collimator unit and is determined from a calibration exposure of unstressed material. It is necessary to measure the distance between at least two lines with known values of diffraction angles or to use an interplanar distance of standard material. Substitution of expression (6) into expression (5) leads to the following expression for the stress calculation:

$$\sigma_\varphi = A(B_2 C_2 - B_1 C_1),$$

where  $A$  is the constant including all known quantities entering in expression (5), such as modulus and diffraction angle.

The principle of stress measurements is shown in Fig. 5. Two cassette windows provide capture of diffraction lines in  $2\theta$  angular intervals, from  $148^\circ$  to  $164^\circ$ . Inclination of the specimen surface

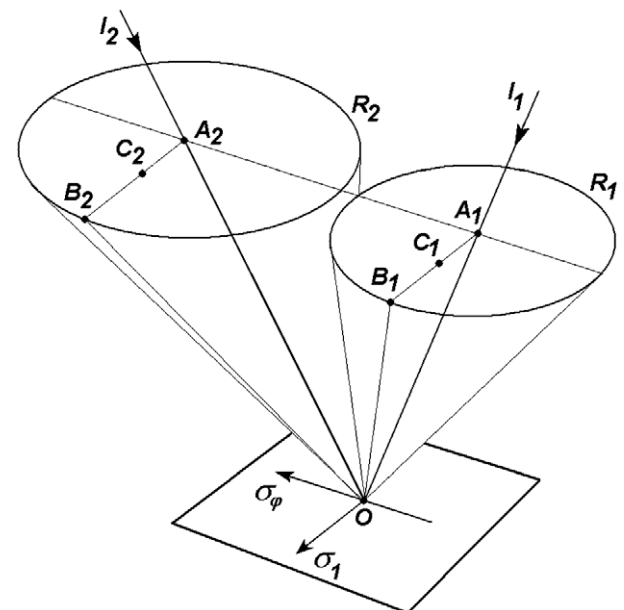


Fig. 4. Scheme of double exposure measurement geometry.

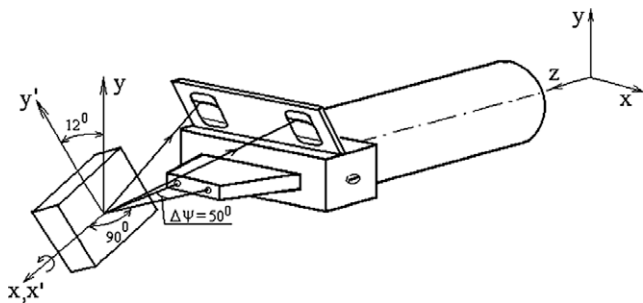


Fig. 5. Scheme of stress measurements with RAYSTRESS equipment.

equal to  $12^\circ$  corresponds to measurement for steel specimen using Cr- $K_\alpha$  radiation and  $\{2\ 1\ 1\}$  reflection with  $\theta_{211} = 78^\circ$ .

Dealing with the X-ray diffraction methods of stress measurements for the welds some authors give special attention to the stress-free lattice spacing. The hypothesis that the change of this lattice spacing across the weld due to microstructural variations affects the results of the stress measurements is explored, for example, in the paper [8]. To adjust the experimental stress measurement results a least squares optimization problem is solved taken unstrained lattice spacing as a control parameter. The optimal solution guarantees that the measured stress is close to the theoretically predicted value on a certain set of measurement points. Then the obtained optimal lattice spacing is used to recalculate stress values for the rest of the measurement points. However, the experimental results [22] show that there is no significant variation of the stress-free lattice spacing, thus we assume here that interplanar distance  $d_0$  does not change across the weld.

#### 4. Results

The residual stress measurements for each pair of joined plates were performed along the mid-plate perpendicular to the weld line at 10 different points (1–10) spaced by 80 mm from each other and from the weld line, as well as at the points at the deposited metal (WM), heat affected zone (HAZ) and base metal close to weld fillet (BM), spaced by 10 mm. The electro-chemical etching to a depth of 0.2 mm was applied to guarantee the absence of mechanical stress induced on the plate surface by manufacturing and collateral procedures and to identify the limits of HAZ. Registration of  $\{2\ 1\ 1\}$  diffraction lines with Cr- $K_\alpha$  wavelength were used for X-ray analysis. The magnitudes of X-ray elastic constants were taken from [23]. The used beam spot size was  $0.5\text{ mm} \times 6\text{ mm}$ . The experimental accuracy of the stress measurements is 20 MPa.

Measurements of the stresses in the plates before welding show the presence of tensile residual stresses, with values between 20 and 40 MPa, caused by thermo-mechanical treatments of the plates during fabrication.

Fig. 6 presents longitudinal and transversal stress values for the single-electrode welding case with all constraints imposed, after the internal constraints removal and after all constraints removal. It is observed the monotonic reduction of the residual stresses while the constraints are gradually removed. Although stresses were reduced almost to zero in the region far from the fillet (points 5–10), before the removal of restrictions the stresses in transversal direction were higher than in longitudinal direction. So the relaxation was more intense for the stresses in the transversal direction. This fact may contribute to increase significantly the angular distortion of the welded plate after removing all welding constraints.

Fig. 7 presents double-electrode welding stress distributions. With all constraints imposed, the maximum values of longitudinal and transversal stresses are observed in the base metal close to

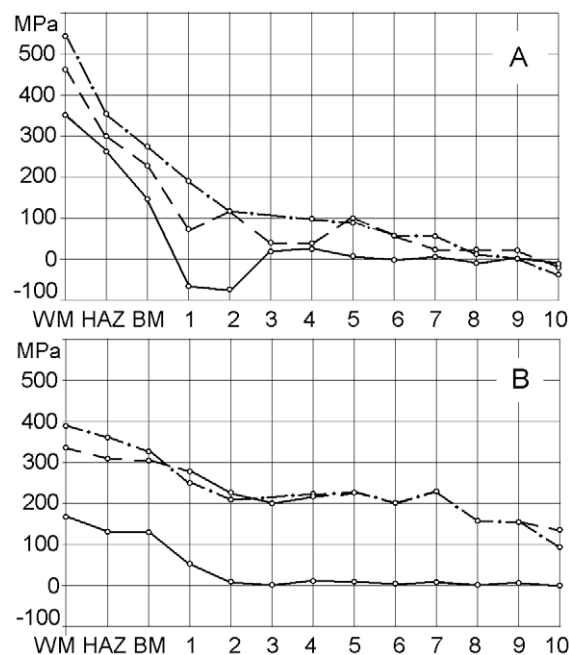


Fig. 6. Surface residual stress for single-electrode welding: all the constraints imposed (dot-and-dash line); internal constraints removed (dash line); all constraints removed (continuous line). (A) Longitudinal stress; (B) transversal stress.

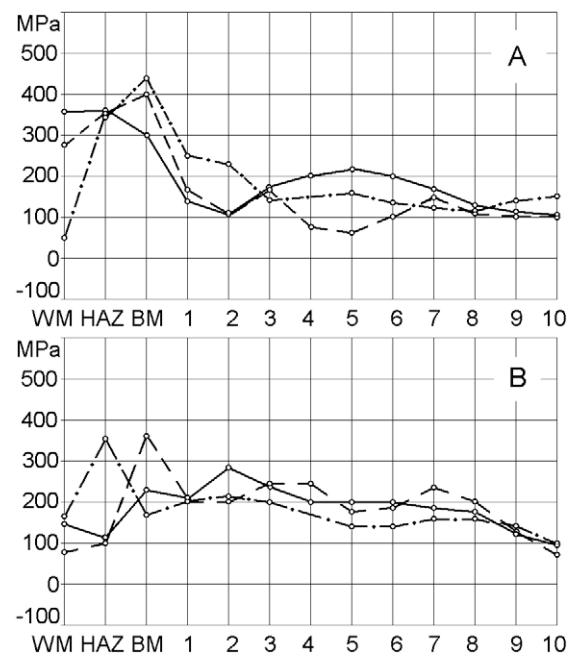


Fig. 7. Surface residual stress for double-electrode welding: all the constraints imposed (dot-and-dash line); internal constraints removed (dash line); all constraints removed (continuous line). (A) Longitudinal stress; (B) transversal stress.

weld fillet and in HAZ area, respectively. When restrictions are gradually removed, the stress reduction in the base metal close to fillet results in increasing of stresses on weld metal in the longitudinal direction. In comparison with the single-electrode behavior, the stresses in this case do not reach the value close to zero at the points remote from the fillet (points 5–10).

It can be clearly noted in the comparison of final stresses for both cases that stress relaxation process is more pronounced in

the single-electrode case. In the double-electrode case stresses remain higher than equivalent values for the single-electrode one, both for longitudinal and transversal directions, Fig. 8. The shape of the stress distribution curve for single-electrode case is in accordance with the classical results for this type of welding [5]. The longitudinal stresses curve decreases from maximum value at the deposited metal to the negative minimum at the point of base metal close to weld fillet (point 2), then increases to positive values (points 3 and 4) and turns to zero (points 5–10). The curve of the measured stress values in longitudinal direction for the double-electrode case has the similar shape with decreasing from maximum at the deposited metal to the minimum at the base metal (point 2) following by increasing to the point 5 and posterior decreasing to the minimum value at the point 10. The fact that the longitudinal and transversal stresses values in double-electrode case are in the interval from 100 to 200 MPa at the points away from the weld fillet (points 4–10) whereas for the single-electrode case the values at these points are close to zero, can be associated with the lower stress relaxation in the double-electrode case.

The out-of-plane distortions of welded plates measured after releasing the constraints are shown in Fig. 9. Measurements of distortions were performed employing the LASER TRACKER equipment. Data were processed in computer-aided design (CAD) software to plot the top side of the plate surface. To compare the distortion measurement results, the support plane considered as zero level was taken in such way that the left and right extreme points of the stop weld plate edge were located at the same elevation. For the double-electrode case, the maximum angular distortion is  $0.34^\circ$ , resulting in 4.74 mm of upward displacement at the plate's corner and maximum bending distortion of 8.86 mm. For the single-electrode case the maximum angular distortion is quite similar, with  $0.30^\circ$  and 4.19 mm, but the maximum bending distortion is much higher, 14.31 mm. Previous numerical simulation results [12] are confirmed by the experiments.

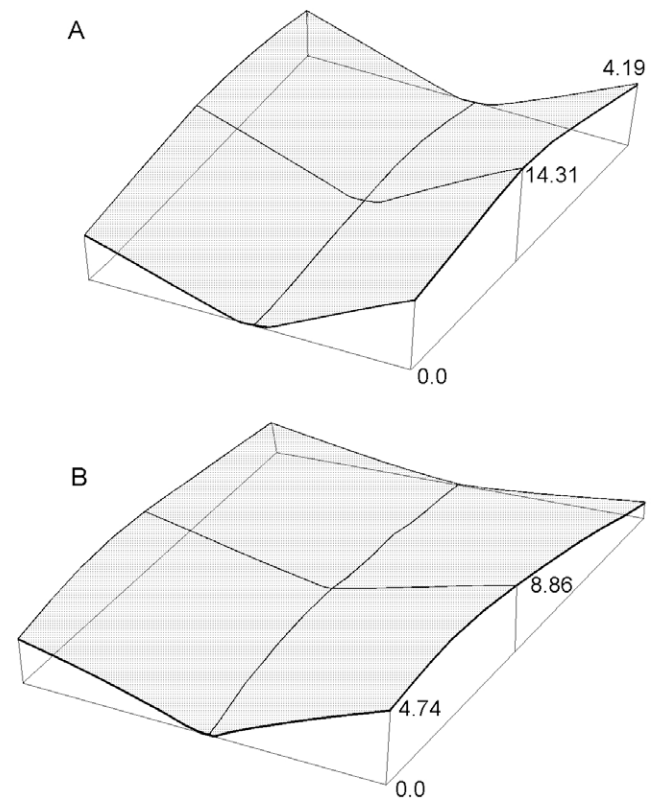


Fig. 9. Surface plotting of butt jointed plates. (A) Single-electrode welding; (B) double-electrode welding. Measurement units - mm.

## 5. Conclusions

By the analysis of the surface residual stress evaluation for double-electrode and single-electrode welding, some conclusions can be derived:

1. Final stresses for the double-electrode case remain higher than equivalent values for single-electrode one, both for longitudinal and transversal directions.
2. Lower values of the bending distortions observed for double-electrode welded plates are in accordance with the smaller welding stress relaxation, compared with the single-electrode case. Moreover, for double-electrode welding the final residual stress distribution is more uniform, especially in the longitudinal direction.
3. For the double-electrode case the initial distribution of maximum welding stress values in both HAZ and base metal close to the fillet, while for the single-electrode case the maximum welding stress values were located along the deposited metal. Similar trends were observed in the other experiments involving double-electrode welding.
4. As a consequence, the welding stress evaluation after the constraints removal in the double-electrode case is in different shape from those obtained for the single-electrode welding. For the single-electrode case the residual stress distribution is a result of the stress redistribution on the deposited metal. For the double-electrode case, the stress reduction in the base metal close to fillet results in increasing of stresses on weld metal in the longitudinal direction.
5. For the double-electrode welded plates the longitudinal residual stresses in the deposited metal remain close to zero only until constraints removal, after that they become compatible with the stress values for the single-electrode case.

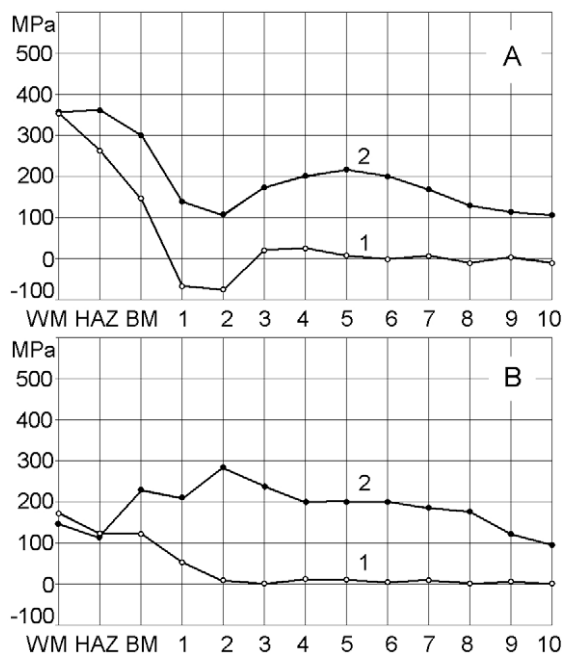


Fig. 8. Surface residual stress final distribution: single-electrode welding (line 1) and double-electrode welding (line 2). (A) Longitudinal stress; (B) transversal stress.

The outlined behaviors of the surface residual stress of double-electrode welding will hopefully be found useful in the practical engineering applications as well as in computational modeling to test the validity of the numerical results.

### Acknowledgments

This work was supported by FINEP/Brazilian Ministry of Science and Technology and TRANSPETRO/PETROBRAS (Contract 0050.0018158.05.4 – “Fabrication Factors in Ship Construction”). The assistance of White Martins S.A. with double-electrode welded specimen fabrication is gratefully acknowledged. Special thanks to the technical team from the Subsea Technology Laboratory – COPPE/UFRJ. The last author (A.L.) gratefully acknowledges the support provided by CNPq (Conselho Nacional de Desenvolvimento Científico e Tecnológico, Brazil; research grant N 308035/2006-2).

### References

- [1] Bajcer B, Hrženjak M, Pompe K, Jež B. Improvement of energy and materials efficiencies by introducing multiple-wire welding. *METABK* 2007;46:47–52.
- [2] Li K, Zhang YM. Metal transfer in double-electrode gas metal arc welding. *J Manuf Sci Eng* 2007;129:991–9.
- [3] Li KH, Zhang YM. Consumable double-electrode GMAW – Part 1: the process. *Weld J* 2008;87:11–7.
- [4] Li KH, Zhang YM, Xu P, Yang FQ. High-strength steel welding with consumable double-electrode gas metal arc welding. *Weld J* 2008;87(Suppl.):S57–87.
- [5] Macherauch E, Wohlfahrt H. Different sources of residual stress as a result of welding. In: Nichols RW, editor. *Residual stress in welded construction and their effects: an international conference*; 1977 Nov 15–17; London. Cambridge: Welding Institute; 1978–1979. p. 267–82.
- [6] Leggatt RH. Residual stress in welded structures. *Int J Pressure Vessel Pip* 2008;85:144–51.
- [7] Okerblom NO. *Welding strains and stresses. Theory and its application*. Moscow: State Scientific-Technical Publishing of Engineering Literature; 1948 [in Russian].
- [8] Korsunsky AM, Regino GM, Nowell D. Variational eigenstrain analysis of residual stresses in a welded plate. *Int J Solids Struct* 2007;44:4574–91.
- [9] Paradowska AM, Price JWH, Finlayson TR, Lienert U, Walls P, Ibrahim R. Residual stress distribution in steel butt welds measured using neutron and synchrotron diffraction. *J Phys: Condens Matter* 2009;21. doi:10.1088/0953-8984/21/12/12421.
- [10] Deng D, Murakawa H. Prediction of welding distortion and residual stress in a thin plate butt-welded joint. *Comput Mater Sci* 2008;43:353–65.
- [11] Pilipenko A. Computer simulation of residual stress and distortion of thick plates in multi-electrode submerged arc welding. Their mitigation techniques. Doctor Thesis. Trondheim: Norwegian University of Science and Technology; 2001.
- [12] Wu CS, Zhang MX, Li KH, Zhang YM. Numerical analysis of double-electrode gas metal arc welding process. *Comput Mater Sci* 2007;39:416–23.
- [13] Monin V, Teodosio JR, Gurova T. A portable X-ray apparatus for both stress measurements and phase analysis under field conditions. *Adv X-ray Anal* 2000;43:66–71.
- [14] Gurova T, Teodosio JR, Rebello JM, Monin V. Study of the residual stress state during plastic deformation under uniaxial tension in a 5.0Cr and 0.5Mo steel. *Scr Mater* 1997;36:1031–5.
- [15] Gurova T, Teodosio JR, Rebello JM, Monin V. Variation of the residual stress state in a welded joint during plastic deformation in a 5.0%Cr and 0.5%Mo steel. *J Strain Anal Eng Des* 1997;32:455–9.
- [16] Gurova T, Teodosio JR, Rebello JM, Monin V. Model for the variation of the residual stress state during plastic deformation under uniaxial tension. *J Strain Anal Eng Des* 1998;33:367–72.
- [17] Monin V, Teodosio JR, Gurova T, Assis J. X-ray study of the inhomogeneity of surface residual stresses after shot-peening treatment. *Adv X-ray Anal* 2000;43:48–53.
- [18] Monin V, Teodosio JR, Gurova T. Study and service control of stress state of high-strength steel cables used in prestressed concrete structures. *Adv X-ray Anal* 2001;44:195–200.
- [19] Monin V, Teodosio JR, Gurova T. Analysis of residual stress state in speed gears for automotive vehicles. *Adv X-ray Anal* 2001;44:187–94.
- [20] Assis JT, Monin V, Teodosio JR, Gurova T. X-ray analysis of residual stress distribution in weld region. *Adv X-ray Anal* 2002;45:225–31.
- [21] Noyan IS, Cohen JB. *Residual stress measurement by diffraction and interpretation*. New York, Berlin: Springer Verlag; 1987.
- [22] Paradowska A, Finlayson TR, Price JWH, Ibrahim R, Steuwer A, et al. Investigation of the samples for residual strain measurements in a welded specimen by neutron and synchrotron X-ray diffraction. *Phys B* 2006;385–386:904–7.
- [23] Hauk V. *Structural and residual stress analysis by nondestructive methods, evaluation–application–assessment*. Amsterdam: Elsevier Science; 1997.